INSTITUTE OF PHYSICS PUBLISHING MEASUREMENT SCIENCE AND TECHNOLOGY
Meas. Sci. Technol. **15** (2004) 1694–1701 PII: S0957-0233(04)78089-3

Broadband characterization of a microwave probe for picosecond electrical pulse measurements

Mark Bieler[1], Meinhard Spitzer[1], Günter Hein[1], Uwe Siegner[1], Frank Schnieder[2], Thorsten Tischler[2] and Wolfgang Heinrich[2]

[1] Physikalisch-Technische Bundesanstalt, Bundesallee 100, D-38116 Braunschweig, Germany
[2] Ferdinand-Braun-Institut für Höchstfrequenztechnik, Albert-Einstein-Strasse 11, D-12489 Berlin, Germany

Received 15 March 2004
Published 23 July 2004
Online at stacks.iop.org/MST/15/1694
doi:10.1088/0957-0233/15/9/004

Abstract
The time-domain characterization of high-frequency devices with coaxial connectors requires the transfer of picosecond electrical pulses between coplanar and coaxial lines. Microwave probes are often used for this purpose. In this paper, the propagation of ultrashort electrical pulses over a microwave probe attached to a coplanar waveguide is experimentally studied by time-domain electro-optic sampling. From the experimental data, the attenuation and dispersion constants of the probe are determined up to 400 GHz. Moreover, the complex reflection and transmission coefficients of the junction between the microwave probe and the coplanar waveguide are extracted. Simple approximations are given for these quantities. These data can be used to predict the amplitude and shape of ultrashort electrical pulses after propagation over the microwave probe for arbitrary input pulses in the considered frequency range.

Keywords: time-domain measurements, electro-optic measurements, transient propagation, coaxial transmission lines, coplanar waveguides

1. Introduction

The time response of high-frequency electronic devices is becoming increasingly important as a result of digital signal processing at ever higher data rates. A reliable determination of the time response requires knowledge of the complex transfer function of the device under test (DUT) even at frequencies well above its 3 dB bandwidth. Nowadays, the 3 dB point of commercially available electronic and optoelectronic devices approaches 100 GHz. Examples include ultrafast pulse generators and photodetectors [1], sampling oscilloscopes with a 3 dB bandwidth of 50 GHz [2], and recently introduced 70 GHz high-speed oscilloscopes. Clearly, such devices need to be characterized at frequencies well above 100 GHz in order to reliably determine their time response. This frequency range is hardly accessible with standard frequency-domain measurements using network analysers. In contrast, time-domain techniques can access this frequency range since their bandwidth extends into the THz range [3, 4]. In essence, due to bandwidth requirements it is often preferable to determine the time response with time-domain measurements.

Time-domain characterization techniques involve optical sampling of ultrashort electrical pulses, which is often based on the electro-optical effect [5, 6]. Electro-optic (EO) sampling can only be applied to planar structures in a straightforward way. Moreover, time-domain characterization often involves optoelectronic generation of ultrashort electrical test pulses, which is usually accomplished with photoconductive (PC) switches embedded in planar transmission lines [7]. Thus, time-domain techniques are established for the characterization of planar devices, such as microstrip lines [8] and coplanar waveguides (CPW) [9].

Yet, high-speed oscilloscopes and ultrafast photodetectors possess coaxial connectors. As a consequence, a method is required that allows one to apply time-domain measurements to coaxial devices. A coaxial–planar link can be constructed for this purpose [10, 11]. This link should allow for the transfer of ultrashort electrical test pulses between the coaxial DUT and the circuit used for the generation or EO detection of the test pulses. For coplanar circuits, such a link can be formed by a microwave probe, which can be attached to a CPW and ends in a coaxial connector. Clearly, the attenuation and dispersion characteristics of the probe have to be known for a reliable characterization of the DUT [11]. To satisfy the bandwidth requirements, the probe characteristics have to be determined well above 100 GHz with picosecond electrical pulses, even though the cut-off frequency of the probe is lower.

In this paper, the propagation of ultrashort electrical pulses over a microwave probe attached to a CPW is experimentally studied by time-domain EO sampling. The attenuation and dispersion of the microwave probe are determined up to 400 GHz from these measurements. Time-domain EO sampling experiments also yield the reflection and transmission coefficients of the junction, which is formed where the microwave probe and the CPW are connected. These measurements provide a complete data set, which allows us to calculate the shape and amplitude of a pulse after propagation over the CPW-probe compound for arbitrary input pulses in the considered frequency range. The output pulses of the CPW-probe compound can be used to determine the time response of, e.g., high-speed oscilloscopes. Simple empirical functions for the propagation quantities were derived to facilitate the description of pulse propagation. We would like to emphasize that only time-domain measurements provide the required bandwidth, even though their uncertainty might be larger than the one of standard frequency-domain techniques.

This paper is organized as follows. In section 2 the experimental set-up is described. The model used for the analysis of the experimental data is introduced in section 3. Section 4 deals with the experimental characterization and the modelling of the CPW, which was performed to validate our experimental procedures. In section 5, we address the measurement of the reflection and transmission coefficients of the CPW-probe junction. Simple calculations of these quantities are presented in the appendix. Finally, the probe attenuation and dispersion are determined in section 6. The results of sections 5 and 6 are used in section 7 to calculate the properties of the pulse at the coaxial end of the microwave probe for a typical input pulse on the CPW. Conclusions are presented in section 8.

2. Experimental set-up

For the generation of ultrashort voltage pulses, we take advantage of non-stoichiometric semiconductors exhibiting a very short carrier trapping time [12]. A 2 μm thick GaAs layer was grown at 210 °C onto a semi-insulating GaAs substrate and subsequently annealed at 690 °C for 20 min. The free carrier trapping time of this material is 1.2 ps, as determined by time-resolved reflectivity measurements. The PC switch itself is incorporated into a CPW, which consists of three 6 mm long

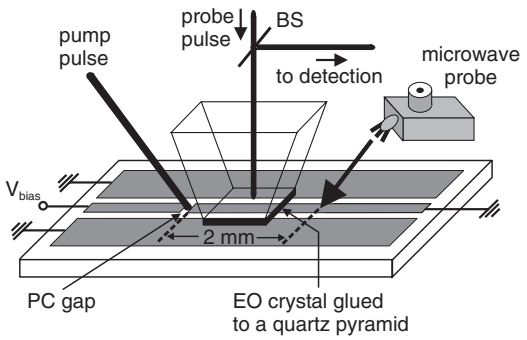

Figure 1. Experimental set-up. PC: photoconductive, EO: electro-optic, BS: beam splitter.

metallic stripes (see figure 1). The stripes were evaporated onto the semiconductor, which had previously been coated with an adhesion layer. The two 500 μm broad ground stripes are separated by 20 μm from the 30 μm broad centre stripe. A 10 μm wide gap in the centre stripe, located 2 mm away from the left end of the CPW, forms the PC switch. In order to generate the voltage pulses, 250 fs laser pulses at 840 nm with an energy of 53 pJ are focused on the centre of the PC gap, which is biased with 20 V. During the measurement, the 500 μm thick semiconductor structure is fixed with silver paint on a copper block.

A 20 μm thick EO crystal ($LiTaO_3$) with an area of $200 \times 200\ \mu m^2$ is placed onto the CPW, at the position where the voltage pulses are to be detected. A second 150 fs laser pulse[3] with an energy of 110 pJ is focused through the EO crystal onto the edge of one ground stripe. The phase of the reflected beam is analysed to detect the electric field-induced refractive index changes. By varying the time delay between the two laser pulses the voltage pulses can be sampled. A lock-in amplifier is used in combination with a differential detector to achieve a good signal-to-noise (S/N) ratio. The experimental set-up allows for the detection of voltages as small as 2 mV (S/N = 2) in a measuring time of 1 s per data point. All experiments are performed at room temperature with 840 nm laser pulses from a 76 MHz titanium:sapphire laser.

To realize the coplanar–coaxial link, a microwave probe (Picoprobe 67A-GSG-50-C) is attached to the CPW 2 mm away from the PC gap, i.e. midway between the gap and the right end of the CPW. The microwave probe ends in a 1.85 mm female coaxial connector and has a cut-off frequency of 67 GHz. The characteristic impedances of the microwave probe and the CPW are 50 Ω at low frequencies. This particular type of microwave probe is chosen for its compatibility with many coaxial DUT. Since many DUT, e.g., oscilloscopes, are equipped with female coaxial input connectors, a male–male adapter is connected to the coaxial end of the microwave probe. In the following analysis, the microwave probe and the male–male adapter are treated as a unit. For characterization, a short termination is attached to the microwave probe. The purpose of the short termination is discussed below.

[3] This laser pulse is shorter than the laser pulse that generates the voltage pulse because the latter one passes through a dispersive acousto-optic modulator.

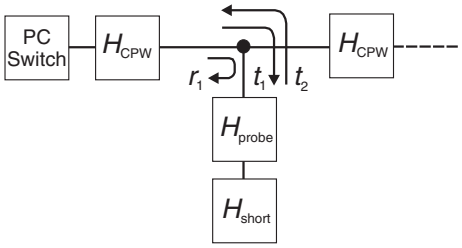

Figure 2. Block diagram of the electrical circuit. PC: photoconductive. H_{CPW}, H_{probe}, H_{short}: complex transfer function of the coplanar waveguide, the microwave probe and the short termination, respectively. t_1, t_2, r_1: transmission and reflection coefficients.

3. Model for data analysis

For the analysis of the experimental data, a simple description is used on the basis of first-order effects. In this regard, we first describe the propagation of the voltage pulses on the CPW–probe compound in more detail. After generation in the PC gap, a picosecond voltage pulse propagates along the CPW towards the CPW–probe junction (forward direction). At the junction it is partially transmitted into the microwave probe. After reflection from the short termination the voltage pulse reaches the junction again. A part of it is transmitted onto the CPW where it propagates towards the PC gap (backward direction). Both the forward propagating (E_{in}) and the backward propagating (E_{out}) voltage pulses are measured by the EO sampling techniques at the same position on the CPW.

We describe the pulse propagation on the CPW by a transmission line model, as is common practice [13]. In this model, a complex transfer function $H_{CPW} = \exp[-(\alpha_{CPW} + j\beta_{CPW})x]$ is introduced, where x is the propagation distance on the CPW, and α_{CPW} and β_{CPW} describe the attenuation and dispersion, respectively. Likewise, the other components of the CPW–probe compound are described in the framework of a transmission line model. The microwave probe is modelled by a complex transfer function $H_{probe} = \exp[-(\delta_{probe} + j\gamma_{probe})]$, where δ_{probe} and γ_{probe} are the attenuation and dispersion constants, respectively. The short termination is described by H_{short}. Since the microwave probe is not attached to the CPW end, a T-junction is formed, as illustrated in figure 2. The junction gives rise to reflections. In the framework of the transmission line model, these reflections are accounted for by complex reflection coefficients and the corresponding transmission coefficients. Figure 2 shows the coefficients that are most relevant for the analysis of our experiments. For propagation from the left end of the CPW to the probe (forward direction), the transmission coefficient is denoted by t_1. Likewise, r_1 is the reflection coefficient in the forward direction. Transmission in the backward direction (from the microwave probe to the CPW) is described by the transmission coefficient t_2. Finally, we introduce a complex transfer function of the total round trip $H_{tot} = \exp[-(\delta_{tot} + j\gamma_{tot})]$, which is obtained from the directly measurable voltage pulses E_{in} and E_{out}. H_{tot} can be expressed as follows:

$$\frac{E_{out}(f)}{E_{in}(f)} = H_{tot} = H_{CPW} t_1 H_{probe} H_{short} H_{probe} t_2 H_{CPW}. \quad (1)$$

Here $E_{out}(f)$ and $E_{in}(f)$ are the Fourier transforms of the time-domain traces $E_{out}(t)$ and $E_{in}(t)$; f denotes the frequency. In order to separate amplitude and phase, we write $t_1 = |t_1| \exp[-j\Phi_1]$ and $t_2 = |t_2| \exp[-j\Phi_2]$ for the complex transmission coefficients in the forward and backward directions, respectively. The transfer function of the short termination is written as $H_{short} = \exp[-j(2l_{offset}\omega/c + \pi)]$; c is the speed of light and $\omega = 2\pi f$ is the angular frequency. The offset length of the short termination $l_{offset} = 7.60$ mm gives rise to a phase term that is linear in the frequency f. The constant π accounts for the phase jump. Here it is assumed that the short termination shows no attenuation and no dispersion. Separating amplitude and phase of (1) yields two new equations:

$$\delta_{tot} = -\ln(|t_1||t_2|) + 2\delta_{probe} + \alpha_{CPW} 2x \quad (2)$$

$$\gamma_{tot} = 2\gamma_{probe} + \beta_{CPW} 2x + (\Phi_1 + \Phi_2) + 2l_{offset}\frac{\omega}{c} + \pi. \quad (3)$$

As mentioned above, δ_{tot} and γ_{tot} (as well as α_{CPW} and β_{CPW}) can be measured directly. With respect to the determination of δ_{probe} and γ_{probe}, we need to comment on the transmission coefficients t_1 and t_2. Figure 2 shows that a forward propagating pulse faces a parallel circuit, formed by the microwave probe and the right end of the CPW. If we replace the parallel circuit by a single impedance, the T-junction reduces to an ordinary junction formed by only two transmission lines. Then, the following relation holds for the reflection and transmission coefficients [14]:

$$t_1 = 1 + r_1. \quad (4)$$

We would like to recall that this expression is generally valid since it only assumes the continuity of voltage and current at the junction. With regard to t_2, a similar analysis of the T-junction shows for arbitrary impedances of the probe and the CPW that the following relation holds (see the appendix):

$$t_2 = -2r_1. \quad (5)$$

The reflection coefficient r_1 can be determined experimentally. Then δ_{probe} and γ_{probe} can be calculated from (2)–(5).

One has to emphasize that this description of the measurement set-up represents only a first approximation. Several phenomena are neglected, which can be expected to cause significant contributions, particularly in the frequency range beyond 70 GHz. In detail, this includes the following two main simplifications: (i) The transmission lines are assumed to be mono-moded (which does not hold for the 1.85 mm coax beyond about 70 GHz) and (ii) the discontinuities and the junction formed by the probe are described using a first-order approach, i.e. by pure transmission-line sections without additional equivalent circuit elements. Within the accuracy range of the measurements, however, this model is found to provide a consistent explanation of the measured data, and a more detailed model would render an interpretation almost impossible. Therefore, for the purpose of the work presented here, the model appears to be justified.

4. Characterization of the CPW

The knowledge of the propagation constants of the CPW is essential for a reliable data analysis. Moreover, CPW measurements can be compared with the established theoretical models to validate the experimental procedures.

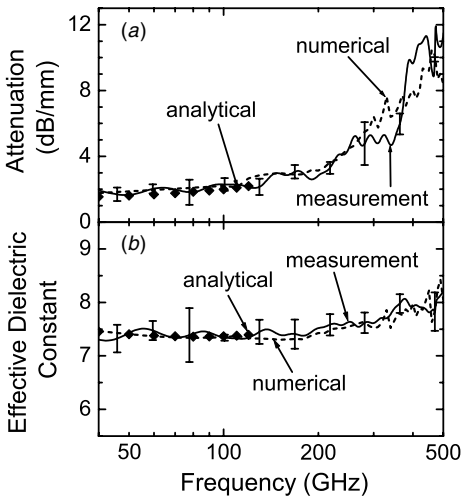

Figure 3. Attenuation α_{CPW} (*a*) and effective dielectric constant $\varepsilon_{\mathrm{eff}}$ (*b*) of the coplanar waveguide. Solid lines: experimental results. The error bars indicate twice the experimental standard deviation for selected frequencies. Dashed lines: finite-difference frequency-domain simulation. Black diamonds: analytical model.

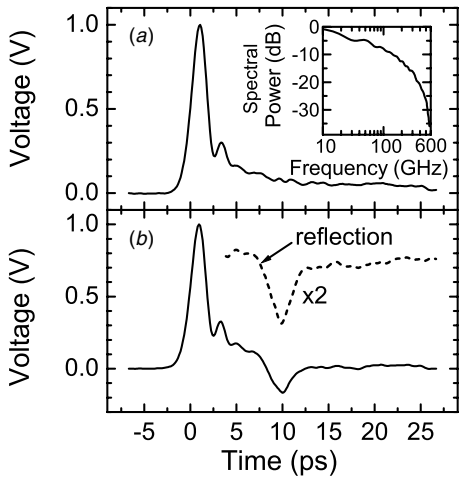

Figure 4. Electro-optic sampling traces. (*a*) Incident pulse on the coplanar waveguide (CPW); microwave probe lifted off. The inset shows the power spectrum. (*b*) Superposition of the incident pulse and the reflection from the junction between the CPW and the microwave probe (solid) and reflection from the junction (dashed, up-shifted by 0.8 V).

For these reasons, we present experimental and theoretical data of the attenuation constant α_{CPW} and the effective dielectric constant $\varepsilon_{\mathrm{eff}} = (\beta_{\mathrm{CPW}} c/\omega)^2$ of the CPW in this section.

The experimental data were derived from an analysis of the shape of two voltage pulses measured at different positions on the CPW spaced by a distance Δx. In this experiment, the microwave probe was lifted off the CPW to avoid reflections. The time traces were Fourier transformed in order to extract α_{CPW} and β_{CPW}. Four independent measurements were performed and the arithmetic means of α_{CPW} and β_{CPW} were calculated. We also calculated the experimental standard deviation of α_{CPW} and β_{CPW} to show how single measurements scatter around the mean [15]. Even though we cannot analyse a very large data set, this procedure substantially improves the experimental data as compared to the single-measurement results, which are usually presented (e.g., [8]). The mean and the experimental standard deviation of $\varepsilon_{\mathrm{eff}}$, which cannot be measured directly, were calculated following the procedure described in [15]. In particular, the mean of $\varepsilon_{\mathrm{eff}}$ is calculated from the mean of β_{CPW}. Figure 3 shows the mean values of α_{CPW} and $\varepsilon_{\mathrm{eff}}$ from 40 GHz to 500 GHz (solid lines). The length of the error bars represents twice the experimental standard deviation at ten different frequency points.

For comparison with the experiment, the attenuation constant α_{CPW} and the effective dielectric constant $\varepsilon_{\mathrm{eff}}$ were calculated using a finite-difference frequency-domain (FDFD) code [16] and a simplified analytical model developed for circuit design [17]. The FDFD method represents a full-wave approach. Radiation losses are included by means of the perfectly matched layer absorbing-boundary condition. Ohmic loss of the metallization and dielectric substrate loss are also taken into account. The analytical model also accounts for all relevant effects: conductor, dielectric and radiation losses, as well as high-frequency dispersion. However, its validity range is restricted to frequencies at which interaction of the CPW mode with higher-order modes can be neglected. These higher-order modes are related to the lateral line dimensions and to the substrate thickness [18]. For the CPW described in section 2, the upper frequency limits imposed by these dimensions are 114 GHz and 121 GHz, respectively. Consequently, the analytical model was only evaluated up to a maximum frequency of 120 GHz. In contrast, the FDFD code can be used at higher frequencies since it also describes the interaction between higher-order modes and the CPW mode. For the given structure, permanent interaction effects occur for frequencies beyond 120 GHz. In this range, the so called co-flow behaviour [19] prevents a clear distinction between the CPW and higher-order modes. This explains the scattering in the simulation data. These effects are parasitic and can be suppressed by an optimized design of the line dimensions, i.e. smaller ground conductor width and reduced substrate thickness.

The calculated values of α_{CPW} and $\varepsilon_{\mathrm{eff}}$ are also shown in figures 3(*a*) and (*b*), respectively, along with the experimental data. Good agreement is found between the experimental results for α_{CPW} and $\varepsilon_{\mathrm{eff}}$ and the results from the analytical and the numerical simulation in the whole frequency range. The good agreement proves that the experimental procedure is reliable. Thus, the data of figure 3 provide a reliable basis for the analysis of pulse propagation over the microwave probe.

5. Characterization of the CPW–probe junction

A transmission line discontinuity is formed where the microwave probe is attached to the CPW. In this section the transmission and reflection coefficients of this junction in the forward (CPW–probe) and backward (probe–CPW) directions are determined experimentally. The experimental results are compared with simple calculations, based on the low-frequency characteristic impedances of the CPW (Z_{CPW}) and the microwave probe (Z_{probe}).

The experiment was carried out as follows. With the probe removed, the incident voltage pulse was sampled 1.5 mm behind the gap. Figure 4(*a*) shows this pulse. The inset displays the spectral power with the 20 dB drop at 500 GHz,

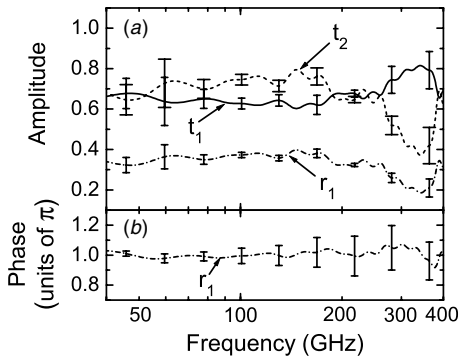

Figure 5. Characterization of the CPW–probe junction. (*a*) Amplitude of the reflection coefficient in the forward direction (r_1, dotted-dashed) and of the transmission coefficients in the forward (t_1, solid) and backward (t_2, dashed) direction. (*b*) Phase of r_1. The error bars indicate twice the experimental standard deviation. The error bars of t_2 have longer cross bars.

i.e. the bandwidth of the incident pulse is large enough for measurements up to 400 GHz. Then the microwave probe was attached to the CPW, 2 mm away from the gap. A second EO sampling measurement was performed at the same position as in the previous experiment, i.e. 0.5 mm away from the CPW–probe junction. The corresponding time trace (figure 4(*b*), solid line) shows a negative contribution around 9 ps after the main pulse, superimposed on the incident pulse. This negative contribution corresponds to the reflection from the CPW–probe junction. The reflection can be extracted subtracting the incident pulse of figure 4(*a*) from the superposition of figure 4(*b*). The result is plotted as the dashed line in figure 4(*b*). The complex reflection coefficient r_1 is obtained by dividing the complex Fourier amplitudes of the reflected pulse by the ones of the incident pulse. The propagation on the CPW is accounted for using the experimental data of figure 3. Four independent measurements were performed, yielding four values of the amplitude and phase of the complex r_1. The means of the amplitude and phase were calculated as well as the experimental standard deviations. The means are plotted in figures 5(*a*) (amplitude) and (*b*) (phase) along with error bars representing twice the experimental standard deviation.

The low-frequency characteristic impedances of the CPW and the probe of 50 Ω give rise to a reflection coefficient $r_1 = -1/3$, see the appendix, (A1). Below 250 GHz the measured amplitude of r_1 does not significantly differ from the value $1/3$ predicted by the low-frequency impedances. This good agreement strongly supports the model outlined in section 3 and the appendix. In this respect, it is important to note that the measurement of r_1 does not rely on the model, i.e. it is a truly independent measurement. Below 250 GHz, the result of this independent measurement agrees with the prediction of the transmission line model if the T-junction is accounted for. The deviations between experimental and theoretical values for r_1 at higher frequencies indicate that Z_{CPW} and/or Z_{probe} differ from their low-frequency values in this range. The phase of r_1 is very close to π over the whole frequency range, in agreement with the prediction for 50 Ω impedances. This result indicates that the imaginary part of Z_{CPW} and Z_{probe} remains much smaller than the real part as the frequency is raised.

The mean amplitude and mean phase of the complex transmission coefficients in the forward (t_1) and backward (t_2) directions were calculated from the mean amplitude and phase of r_1 with (4) and (5). The experimental standard deviations were computed following [15]. The amplitudes of t_1 and t_2 are shown in figure 5(*a*). Again, error bars indicate twice the experimental standard deviation. For 50 Ω impedances one obtains $|t_1| = |t_2| = 2/3$. The experimental results for $|t_1|$ and $|t_2|$ show no substantial deviation from this prediction up to frequencies of 250 GHz. At higher frequencies the experimentally determined $|t_2|$ deviates more strongly from $2/3$. This result can be expected from the behaviour of $|r_1|$ and the proportionality between $|r_1|$ and $|t_2|$. The amplitude $|t_1|$ does not significantly differ from $2/3$ in the whole frequency range if the error bars are taken into account. This result does not contradict the behaviour of $|r_1|$ but merely reflects that $|t_1|$ depends less sensitively on $|r_1|$ than $|t_2|$ due to the different relations (4) and (5). Figure 5(*a*) also shows that $|t_1|$ and $|t_2|$ differ from each other at higher frequencies. This finding is not surprising since t_1 and t_2 are equal if and only if the impedances of the CPW and the probe are equal (see the appendix). This statement does not contradict the reciprocity theorem for scattering matrices since the scattering matrix formalism considers power waves while the transmission coefficients connect voltage waves. Finally, we note that the phases of t_1 and t_2 are very close to zero (0 ± 0.26 rad) over the whole frequency range. As these phases do not contain new information, they are not shown.

6. Characterization of the microwave probe

With the results of sections 4 and 5 we are now in a position to characterize the microwave probe. For this purpose, the total transfer function H_{tot} was determined from the measurements of the forward and backward propagating pulses at the same position between the gap and the microwave probe. The probe is attached to the CPW 2 mm away from the gap.

First, we focus on the attenuation. From four independent measurements the mean of δ_{tot} and its experimental standard deviations were calculated. Subsequently, the mean of δ_{probe} was computed using (2). Its experimental standard deviation was determined according to [15]. In figure 6(*a*) the means of the attenuation constants δ_{tot} and δ_{probe} are plotted along with twice the experimental standard deviation as error bars. We only discuss the probe attenuation in the following since δ_{tot} is an auxiliary quantity. The probe attenuation is small in the frequency range up to 150 GHz while it strongly increases from 150 GHz to 210 GHz. Above 210 GHz resonances are observed, which we attribute to the excitation of higher modes in the coaxial line. The filled diamond at 67 GHz was determined with frequency-domain methods by the manufacturer of the probe. This data point and our measurement differ by less than the standard deviation, strongly supporting our experimental procedures and the model used for the data analysis.

We now address the phase measurements. The phase data consist of two terms: a term that is linear in the frequency f and a nonlinear term. The linear term contains information on the absolute propagation time while the nonlinear term describes the distortion of a propagating pulse due to

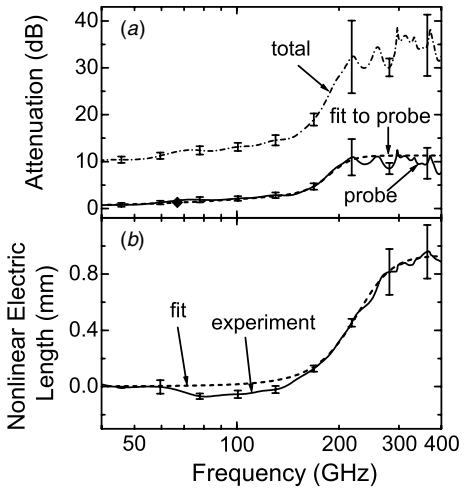

Figure 6. Characterization of the microwave probe. (*a*) Experimentally determined total (dotted-dashed) and probe (solid) attenuation. Dashed: fit to probe attenuation. (*b*) Nonlinear electric length L_{NL} of the microwave probe. Solid: experimental data. Dashed: fit. The error bars indicate twice the experimental standard deviation of the experimental data.

dispersion. In many applications, one is only interested in how the DUT changes the shape of the test pulse. The absolute propagation time of the test pulse does not have to be known in this situation. Consequently, the linear phase term of the microwave probe is irrelevant in many applications. Therefore, we restrict ourselves to the analysis of the nonlinear term, which determines the shape of the test pulse.

In view of the above, the phase data were processed differently than the attenuation data. From the four independent measurements of $H_{\mathrm{tot}}(f)$ and $\gamma_{\mathrm{tot}}(f)$, four independent $\gamma_{\mathrm{probe}}(f)$ curves were calculated using (3). Subsequently, we extract the linear part of each of these curves from fits with the function $2\pi f T_0$ in the frequency range from 40 GHz to 50 GHz. The constant T_0 is the low-frequency propagation time determined independently from each $\gamma_{\mathrm{probe}}(f)$ curve. Subtracting $2\pi f T_0$ from $\gamma_{\mathrm{probe}}(f)$ yields the nonlinear phase $\gamma_{\mathrm{probe,NL}}(f)$ of the microwave probe for each of the four measurements. Finally, the mean and the experimental standard deviation of $\gamma_{\mathrm{probe,NL}}(f)$ are computed. To present a quantity that is more widely used in microwave technology, we plot the nonlinear electric length L_{NL} in figure 6(*b*), defined as $L_{\mathrm{NL}} = \gamma_{\mathrm{probe,NL}} c/\omega$. The solid curve represents the mean while the error bars indicate twice the experimental standard deviation. The nonlinear electric length is nearly zero up to 150 GHz and increases at higher frequencies, showing that the microwave probe becomes dispersive for frequencies above 150 GHz.

Figure 6 contains the information that is needed to calculate the shape of test pulses after propagation over the microwave probe for input pulses whose bandwidth does not extend beyond 400 GHz. In this frequency range, the data of figure 6 provide a solid basis for the characterization of coaxial devices with time-domain sampling methods if the microwave probe is used as a coplanar–coaxial link. To make the information of figure 6 more readily accessible, we approximated $\delta_{\mathrm{probe}}(f)$ and $L_{\mathrm{NL}}(f)$ with empirical functions. These functions were obtained from fits in the frequency range from 40 GHz to 400 GHz. The fits yield

$$\delta_{\mathrm{probe}} = 1.3 - \frac{0.35}{1+\exp\left[\frac{f/\mathrm{GHz}-80}{36}\right]} - \frac{0.95}{1+\exp\left[\frac{f/\mathrm{GHz}-186}{15}\right]} \tag{6}$$

$$L_{\mathrm{NL}} = 0.93\left(1 - \frac{1}{1+\exp\left[\frac{f/\mathrm{GHz}-220}{30}\right]}\right)\ \mathrm{mm}. \tag{7}$$

The empirical functions are plotted in figures 6(*a*) and (*b*) as dashed lines. Good agreement with the measured data is obtained in the frequency range from 40 GHz to 400 GHz. In the next section, we calculate an example of pulse propagation over the microwave probe in which the empirical functions (6) and (7) are used in the whole frequency range from zero to 400 GHz. It is shown that there is hardly any difference between output pulses calculated with the empirical functions (6) and (7) and output pulses calculated with the experimental attenuation and dispersion data. Thus, we conclude that the empirical functions (6) and (7) can be used at frequencies $0 \leqslant f \leqslant 400$ GHz.

7. Propagation of ultrashort voltage pulses

In this section, we demonstrate the usefulness of the microwave probe characterization of sections 5 and 6. As an example of the practical impact of this work, we calculate the shape of a test pulse at the coaxial end of the microwave probe for a given input pulse on the CPW. This task is often encountered if devices with coaxial input are to be characterized. A typical example is the measurement of the risetime of high-speed oscilloscopes [2]. In particular, we show that simple approximations of the experimental microwave probe data can be used to facilitate the calculations.

Figure 7(*a*) shows the input pulse $E_{\mathrm{test}}(t)$ that we have chosen for the calculation. Such pulses are routinely obtained after 2 mm propagation on the CPW. In order to treat the effect of the microwave probe unperturbed by CPW effects, it is assumed that the input pulse of figure 7(*a*) is incident directly on the CPW–probe junction without any further propagation on the CPW. The power spectrum in the inset of figure 7(*a*) shows that the spectral power drops to 29 dB at 400 GHz. Therefore, we can neglect frequency components above 400 GHz. The experimental results of the previous sections, which were obtained up to a maximum frequency of 400 GHz, are then sufficient. With respect to the low-frequency part of the spectrum (dc to 40 GHz), one should note that the experimental data from time-domain sampling show relatively large relative standard deviations in this frequency range[4]. For this reason, the low-frequency data were not shown in the previous sections. In fact, below 40 GHz more accurate measurements could be obtained with standard frequency-domain measurements. Fortunately, however, the probe attenuation and the nonlinear phase of the probe are very small below 40 GHz. As a consequence, variations of these quantities in the low-frequency range do not substantially affect the calculations. Moreover, in general, the shape of

[4] The time-domain measurements were performed over a limited time window of 25 ps due to experimental reasons. Consequently, one only obtains very accurate data in the frequency domain for frequencies larger than 40 GHz.

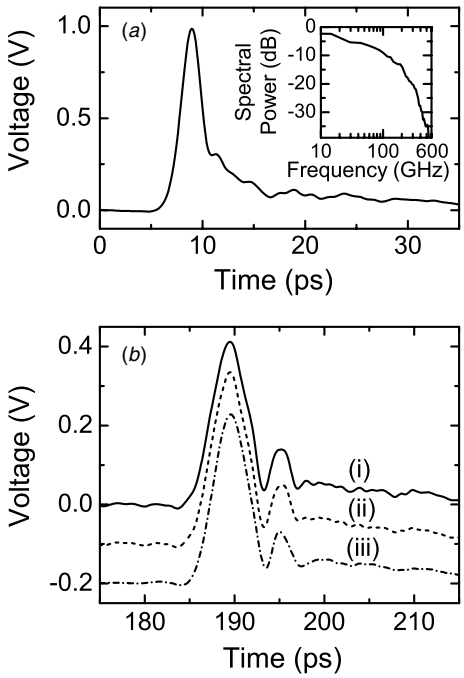

Figure 7. (*a*) Electro-optic sampling trace of the input pulse used to calculate the pulse at the coaxial end of the microwave probe. Inset: power spectrum of the input pulse. (*b*) Voltage pulse at the coaxial end of the microwave probe calculated with (i) only experimental quantities; (ii) experimental propagation quantities and $t_1 = 2/3 = \text{const.}$; (iii) empirical functions to describe the microwave probe and $t_1 = 2/3 = \text{const}$. For clarity, (ii) and (iii) are down-shifted by 0.1 V and 0.2 V, respectively.

ultrafast voltage signals mainly depends on the high-frequency part of the spectrum. Therefore, propagation and transmission constants do not have to be known very exactly below 40 GHz. For these reasons, reliable calculations can be performed that involve the low-frequency experimental data, even though their relative standard deviation is relatively large.

Figure 7(*b*) shows the output pulses $E_c(t)$ at the coaxial end of the microwave probe, obtained from

$$E_c(f) = \exp(-\delta_{\text{probe}}(f)) \times \exp(-j\omega(L_{\text{NL}}(f)/c + T_0))t_1(f)E_{\text{test}}(f). \quad (8)$$

The low-frequency propagation time over the microwave probe T_0 was set to 180 ps, accounting for the experimental results of the previous section. The solid curve in figure 7(*b*) with a full width at half maximum (FWHM) of 4.7 ps was calculated using only experimental data. The dashed curve was obtained replacing the experimentally determined complex transmission coefficient $t_1(f)$ by the constant 2/3, which is the value expected for $Z_{\text{CPW}} = Z_{\text{probe}} = 50\ \Omega$. For clarity, the curve is down-shifted by 0.1 V. The dashed curve can hardly be distinguished from the solid one. In particular, the same FWHM of 4.7 ps is obtained. This result justifies the replacement of $t_1(f)$ by the constant 2/3, which greatly facilitates the determination of the pulse shape at the coaxial connector [20].

In a third step, the experimentally determined $\delta_{\text{probe}}(f)$ and $L_{\text{NL}}(f)$ were replaced by the empirical functions (6) and (7), respectively, in addition to setting $t_1 = 2/3 = \text{const}$. The resulting pulse shape is plotted as a dotted-dashed curve in figure 7(*b*), down-shifted by 0.2 V for clarity. It has a FWHM of 4.5 ps, very close to the values obtained previously, and its shape is almost identical to the other curves. Figure 7(*b*) demonstrates that the empirical functions (6) and (7) provide a simple means for the calculation of picosecond pulse propagation in practically relevant cases.

8. Conclusions

We determined the complex transfer function of a microwave probe experimentally up to frequencies of 400 GHz with time-domain sampling techniques. These results are relevant for measurements of the time response of coaxial devices with time-domain techniques. In these applications, ultrashort electrical test pulses have to be transferred between a coplanar pulse generator or coplanar detection circuit and the coaxial device under test. For this purpose, microwave probes are often used. Our experimental results allow one to calculate the shape of ultrashort test pulses after propagation over the microwave probe. This task is facilitated by the simple empirical functions for the microwave probe propagation constants derived in this paper.

Acknowledgment

The authors would like to thank T Schrader and U Arz for useful discussions, and H Lecher for expert technical assistance. The non-stoichiometric GaAs was grown by P Specht and E R Weber, University of California at Berkeley, supported by the AFOSR grant F49620-01-1-0151.

Appendix

The T-junction formed by the microwave probe attached to the CPW represents a transmission line discontinuity with reflection and transmission coefficients. In the forward direction, the microwave probe and the right end of the CPW form a parallel circuit. Assuming continuity of current and voltage at the junction, it follows for the reflection coefficient in the forward direction, r_1 (compare with figure 2):

$$r_1 = \frac{(Z_{\text{CPW}} \| Z_{\text{probe}}) - Z_{\text{CPW}}}{(Z_{\text{CPW}} \| Z_{\text{probe}}) + Z_{\text{CPW}}} = -\frac{1}{1 + 2\frac{Z_{\text{probe}}}{Z_{\text{CPW}}}}, \quad (A1)$$

where $\|$ denotes 'parallel to'. We would like to emphasize that Z_{CPW} and Z_{probe} are the characteristic impedances of the CPW and the microwave probe, respectively ($Z_{\text{CPW}} = Z_{\text{probe}} = 50\ \Omega$ at low frequencies). Multiple reflections are not superimposed in time in our pulsed experiments and, therefore, an impedance transformation does not have to be performed. From r_1 the transmission coefficient in the forward direction, t_1, is easily calculated:

$$t_1 = 1 + r_1 = \frac{2\frac{Z_{\text{probe}}}{Z_{\text{CPW}}}}{1 + 2\frac{Z_{\text{probe}}}{Z_{\text{CPW}}}}. \quad (A2)$$

In the backward direction (from the microwave probe to the CPW), the two ends of the CPW form a parallel circuit. In this case, the reflection coefficient r_2 is expressed by

$$r_2 = \frac{(Z_{\text{CPW}} \| Z_{\text{CPW}}) - Z_{\text{probe}}}{(Z_{\text{CPW}} \| Z_{\text{CPW}}) + Z_{\text{probe}}} = \frac{1 - 2\frac{Z_{\text{probe}}}{Z_{\text{CPW}}}}{1 + 2\frac{Z_{\text{probe}}}{Z_{\text{CPW}}}} \quad (A3)$$

and

$$t_2 = 1 + r_2 = \frac{2}{1 + 2\frac{Z_{\text{probe}}}{Z_{\text{CPW}}}} = -2r_1. \qquad \text{(A4)}$$

Thus, both t_1 and t_2 can be calculated from the experimentally determined r_1. We would like to note that $t_1 = t_2$ implies $Z_{\text{CPW}} = Z_{\text{probe}}$, compare (A2) and (A4). Moreover, for $Z_{\text{CPW}} = Z_{\text{probe}}$ one immediately finds $t_1 = t_2 = 2/3$.

References

[1] Clement T S, Williams D F, Hale P D and Morgan J M 2002 Calibrating photoreceiver response to 110 GHz *15th Ann. Meeting of the IEEE Lasers and Electro-Optics Society Digest, 2002*

[2] Smith A J A, Roddie A G and Henderson D 1996 Electrooptic sampling of low temperature GaAs pulse generators for oscilloscope calibration *Opt. Quantum Electron.* **28** 933–43

[3] Valdmanis J A 1987 1 THz-bandwidth prober for high-speed devices and integrated circuits *Electron. Lett.* **23** 1308–10

[4] Wu Q and Zhang X-C 1997 7 terahertz broadband GaP electro-optic sensor *Appl. Phys. Lett.* **70** 1784–6

[5] Valdmanis J A and Mourou G A 1986 Subpicosecond electrooptic sampling: principles and applications *IEEE J. Quantum Electron.* **22** 69–78

[6] Kolner B H and Bloom B M 1986 Electrooptic sampling in GaAs integrated circuits *IEEE J. Quantum Electron.* **22** 79–93

[7] Auston D H 1975 Picosecond optoelectronic switching and gating in silicon *Appl. Phys. Lett.* **26** 101–3

[8] Heiliger H-M, Nagel M, Roskos H G, Kurz H, Schnieder F, Heinrich W, Hey R and Ploog K 1997 Low-dispersion thin-film microstrip lines with cyclotene (benzocyclobutene) as dielectric medium *Appl. Phys. Lett.* **70** 2233–5

[9] Frankel M Y, Gupta S, Valdmanis J A and Mourou G A 1991 Terahertz attenuation and dispersion characteristics of coplanar transmission lines *IEEE Trans. Microwave Theory Tech.* **39** 910–6

[10] Bieler M, Spitzer M, Hein G and Siegner U 2002 Time-domain characterisation of non-coplanar high-frequency components up to 300 GHz *Electron. Lett.* **38** 1038–9

[11] Smith A J A, Roddie A G and Woolliams P D 2000 Electro-optic sampling of coplanar to coaxial transitions to enhance the calibration of fast oscilloscopes *56th IEEE ARFTG Conf. (Boulder, CO)*

[12] Whitaker J F 1993 Optoelectronic applications of LTMBE III–V materials *Mater. Sci. Eng.* B **22** 61–7

[13] Gupta K C, Garg R and Bahl I J 1979 *Microstrip Lines and Slot Lines* (Norwood, MA: Artech House)

[14] Pozar D M 1998 *Microwave Engineering* (New York: Wiley)

[15] Guide to the Expression of Uncertainty in Measurement 1993 *International Organization for Standardization (Geneva, Switzerland)*

[16] Tischler T and Heinrich W 2000 The perfectly matched layer as lateral boundary in finite-difference transmission-line analysis *IEEE Trans. Microwave Theory Tech.* **48** 2249–53

[17] Schnieder F, Tischler T and Heinrich W 2003 Modeling dispersion and radiation characteristics of conductor-backed CPW with finite ground width *IEEE Trans. Microwave Theory Tech.* **51** 137–43

[18] Heinrich W, Schnieder F and Tischler T 2000 Dispersion and radiation characteristics of conductor-backed CPW with finite ground width *Int. Microwave Symp. Digest* pp 1663–6

[19] Shigesawa H H, Tsuji M and Oliner A A 1990 A new mode-coupling effect on planar waveguides of finite width *Int. Microwave Symp. Digest* pp 1063–6

[20] Bieler M, Spitzer M, Lecher H, Hein G and Siegner U 2002 Transfer of sub-5 ps electrical test pulses to coplanar and coaxial structures *Electron. Lett.* **38** 125–6